Pre-equilibrium stopping and charge capture in proton-irradiated aluminum sheets

Alina Kononov

Department of Physics, University of Illinois at Urbana-Champaign, Urbana, Illinois 61801, USA

André Schleife [*]

Department of Materials Science and Engineering, University of Illinois at Urbana-Champaign, Urbana, Illinois 61801, USA;
Materials Research Laboratory, University of Illinois at Urbana-Champaign, Urbana, Illinois 61801, USA;
and National Center for Supercomputing Applications, University of Illinois at Urbana-Champaign, Urbana, Illinois 61801, USA

We present a first-principles study of pre-equilibrium stopping power and projectile charge capture in thin aluminum sheets irradiated by 6–60 keV protons. Our time-dependent density functional theory calculations reveal enhanced stopping power compared to bulk aluminum, particularly near the entrance layers. We propose the additional excitation channel of surface plasma oscillations as the most plausible explanation for this behavior. We also introduce a technique to compute the orbital-resolved charge state of a proton projectile after transmission through the sheet. Our results provide insight into the dynamics of orbital occupations after the projectile exits the aluminum sheet and have important implications for advancing radiation hardness and focused-ion beam techniques, especially for few-layer materials.

I. INTRODUCTION

Although ion irradiation represents a fundamental means of manipulating materials and probing their properties [1–6], a detailed theoretical understanding of the interaction between an energetic charged particle and induced electronic excitations in a solid has proven challenging. The Bethe formula [7,8] models electronic stopping power $S = -dE/dz$ (i.e., the energy deposited per penetration depth) for fast projectiles, while the Fermi-Teller model [9] applies to slow projectiles. The Lindhard stopping formula [10] from linear-response theory and its extensions [11] accurately account for the small electron density perturbations produced by fast, low-Z projectiles. However, these existing analytical models [7–11] rely on ambiguous parameters such as projectile charge Z or participating electron density n which not only have multiple meaningful definitions but may also evolve dynamically during the projectile's transit [12].

In addition, upon entering the material, quantities such as stopping power and the projectile's charge state are not initially identical to the steady-state bulk values presumably achieved as the projectile moves through a thick target [13]. This leads to pre-equilibrium effects that cannot be ignored when understanding electronic stopping near surfaces or in thin target materials of only a few atomic layers. In these, the projectile may not reach an equilibrium charge state at all, since it may need to traverse many layers before doing so [13]. While pre-equilibrium effects should occur even for light ions, they should be most prominent for highly charged projectiles

with a large difference between initial and equilibrated charge state.

Indeed, several experiments on highly charged ions impacting carbon-based materials with thicknesses of only a few nm or less reported that the projectile's initial charge influences energy and charge transfer distributions [14,15] and even material damage characteristics [3,16]. Similarly, the response of aluminum foils to ion irradiation has been shown to depend on both ion charge and foil thickness [17,18]. Such studies inferred projectile charge equilibration time scales smaller than 10 fs and length scales shorter than 10 nm [14,16,18–20]. Sensitivity of electron emission to incident ion charge was shown even for ∼100 nm thick carbon foils and attributed to pre-equilibrium stopping and projectile charge [21].

These experimental observations of pre-equilibrium effects inspired exponential decay models for projectile charge equilibration [14,18]. Since experiments cannot access the projectile's charge state within the material, studies evaluating such models typically compare their predictions to measurements of the projectile's charge after transmission through the sample [14,20]. However, this exit charge state may not be equivalent to the projectile's charge state inside the material. Overall, the transition and equilibration of the ion into the bulk regime is still poorly understood and requires further study.

Conversely, for bulk materials under ion irradiation, stopping power has been fairly well-studied experimentally [22–24]. In addition, modern first-principles simulations have provided a detailed description of the energy and charge dynamics in bulk, as evident from many recent studies of electronic stopping power in metals [25–29], semiconductors [13,30–35], and insulators [36–38] which were enabled by the rise of high performance computing. However, it remains difficult for experiments to access the poorly understood

[*]schleife@illinois.edu

pre-equilibrium behavior of stopping power near a surface or for materials thinner than the length scale of projectile charge equilibration.

To improve our understanding of pre-equilibrium behavior, computational modeling of thin materials under ion irradiation is a promising alternative, as it offers greater spatial and temporal resolution than currently achievable experimentally. However, modeling an ion's interaction with a surface requires the inclusion of a sufficiently large vacuum region and sufficiently large material surface, greatly increasing computational cost. In addition, extracting observables from the simulated time-dependent electron density to describe the charge dynamics instigated by ion-induced electronic excitations presents a further challenge. Since detailed understanding of pre-equilibrium behavior is currently absent, we aim to study these effects in the present work.

To this end, we used a first-principles computational approach to calculate and analyze electronic stopping and projectile charge state as protons traverse aluminum sheets. We focus on protons with velocities of 0.5–1.5 at. u. (kinetic energies of 6–60 keV) that move along a channeling trajectory through 15–46 a_0 (0.8–2.4 nm) of aluminum, corresponding to 4–12 atomic layers. The wealth of existing literature on the electronic response of bulk aluminum to proton irradiation makes this an ideal system to study dynamical behavior near ion-irradiated surfaces. In particular, the stopping power of protons in bulk aluminum has been studied extensively both experimentally [22–24] and theoretically [25,26,39–41]. This existing wisdom provides opportunities both to validate our results for the bulk limit and to clearly identify surface effects and pre-equilibrium behavior. Moreover, light-ion irradiation is particularly well-suited for first-principles studies because they experience relatively little scattering in the host material, resulting in long, straight trajectories [1]. Using a proton projectile further allows us to accurately calculate the charge captured by the projectile using analytic hydrogen orbitals, as we discuss below.

The remainder of this paper is structured as follows: In Sec. II we outline the first-principles computational approach used here, and in Sec. III we describe the post-processing methods developed and used to extract projectile charge capture and sheet dipole moment from time-dependent electron density data. Section IV presents the results obtained for pre-equilibrium stopping power and charge capture, and Sec. V summarizes the conclusions drawn from this study.

II. COMPUTATIONAL METHODS

We used real-time time-dependent density functional theory (TDDFT) [42–46] as implemented [26,47,48] in the Qbox/Qb@ll code [49,50] to simulate the real-time nonadiabatic electron-ion dynamics as a proton traverses thin aluminum sheets. Different sheet thicknesses consisting of 4–12 atomic layers were studied, where one layer corresponds to about 3.8 a_0 (0.2 nm) and a_0 is the Bohr radius. The Kohn-Sham (KS) orbitals were expanded in a plane-wave basis with a cutoff energy of 50 Ry. The electron-ion interaction was described using a Troullier-Martins pseudopotential [51] with 11 valence electrons for aluminum and a Hamann-Schlüter-Chiang-Vanderbilt pseudopotential [52] for the proton

projectile. The large simulation cells used in this work, typically $38 \times 38 \times 150\, a_0^3$, allow reciprocal-space sampling using the Γ point only. The adiabatic local density approximation [53,54] was used to describe exchange and correlation. The electronic ground state of the aluminum sheet served as the initial condition of the time-dependent calculations, and it was computed using density functional theory with 100 empty states and a Fermi electron temperature of 100 K in order to accelerate self-consistent convergence of the metallic ground state.

Due to the few-fs time scale of our time-dependent simulations, ions do not have enough time to respond to the forces they experience. Thus, we fix the positions of the aluminum ions and maintain a constant velocity of the proton projectile. The proton starts at a distance of at least 25 a_0 from the aluminum sheet and traverses it along a [100] channeling trajectory (see Fig. 1). The enforced time reversal symmetry (ETRS) integrator [56,57] with a time step of 0.042 at. u. (1.04 as) was used to propagate the Kohn-Sham orbitals, a choice shown to produce high numerical accuracy for similar systems [34]. The cutoff energy, treatment of semicore electrons, target atom dynamics, and channeling projectile trajectory used in this work are identical to those in Ref. [26], where they were shown to produce accurate stopping power results for proton-irradiated bulk aluminum within the velocity regime presently considered. We address accuracy of the time propagation and convergence with respect to supercell size for these large simulation cells in Sec. SI and Sec. SII of Ref. [58]. From our real-time TDDFT simulations we obtain time-dependent electron densities which we analyze further using the approaches discussed in the following section.

III. ELECTRON DENSITY ANALYSIS

It is a central goal of this work to quantify and analyze the charge state of the projectile both inside and outside the aluminum target material. Information about the projectile's charge state could be estimated by analyzing coefficients of the KS orbitals in an atomic orbital basis [36,59–62], by projecting the KS orbitals onto atomic orbitals [63], or by considering probabilities that the KS orbitals are localized within a given volume of interest [64–68]. However, many of these methods have well-known shortcomings, most notably that they rely directly on the single-particle, noninteracting KS orbitals which have no rigorous physical meaning.

Instead, a method that provides the projectile charge state as a functional of only the total electron density—a real, physical quantity which, in principle, determines all observables [42]—would be preferable. Existing methods that extract atomic charges directly from the electron density typically rely on volume [69] or charge [70,71] partitioning, which either assume a definite boundary between the captured electrons and nearby free electrons or neglect free electrons altogether. In this context, we apply the DDEC6 [70,71] charge partitioning method in this work to calculate the effective projectile charge state as the proton traverses the aluminum sheet. However, this technique is not applicable in the presence of free electrons and, hence, we find that it overestimates the number of electrons bound to the projectile
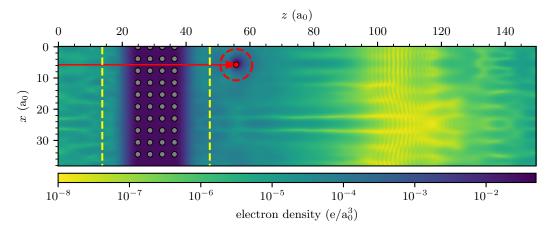
FIG. 1. Illustration of our simulation cell at a time of 0.75 fs after a proton with a velocity of 1 at. u. impacts a four-layer thick aluminum sheet. A slice of the electron density is overlaid with projected positions of aluminum atoms in gray and the projectile along with its trajectory in red. Electron density has been emitted into the vacuum and captured by the projectile. Dashed yellow lines indicate the aluminum-vacuum boundaries used for calculating the sheet's dipole moment, and the 5 a_0 projectile radius [55] used to compare our charge capture method with volume partitioning is indicated by the red dashed circle (see Sec. III of this paper and Sec. SIII of Ref. [58]).

once it emerges from the material into the vacuum containing emitted electrons (see Fig. S6 of Ref. [58]).

Since the electron distribution emitted into vacuum, not including those captured by the projectile, should not be assigned to any atoms, a different method is required to calculate charge captured by the projectile after traversing the material. Once the projectile has left the target material, a common strategy simply integrates the electron density within a sphere centered at the projectile [38,55,72–76]. However, the radius chosen for this sphere (for instance, 5 a_0 in Ref. [55]) defines an artificial, discrete boundary between electrons captured by the projectile and free electrons in the vacuum which, depending on the radius chosen and the occupied projectile orbitals, could either falsely include emitted electrons or falsely exclude higher energy captured electrons.

Instead, we present a physically motivated method of calculating the charge captured by a proton and also the orbital distribution of the captured charge as a functional of the electron density. We first obtain the radial distribution $n(r, t)$ of the electron density around the projectile, in units of e/a_0, by integrating the electron density $n(\mathbf{r}, t)$ over spherical shells S,

$$n(r, t) = \frac{1}{\Delta r} \int_{S(r, \mathbf{R}(t))} n(\mathbf{r}, t) \, dr^3. \quad (1)$$

Here, Δr is the smallest real-space grid spacing in each simulation and $S(r, \mathbf{R}(t))$ is the spherical shell of thickness Δr and radius r, centered at the projectile's position $\mathbf{R}(t)$. Integrating $n(r, t)$ from Eq. (1) again over r would give the number of electrons within a sphere around the projectile. Using the electron densities from our simulations, represented on a real-space grid, we evaluate the following discrete version of Eq. (1) to compute $n(r, t)$:

$$n(r_i, t) = \frac{1}{\Delta r} \sum_{r_{i-1} < |\mathbf{r} - \mathbf{R}(t)| \leqslant r_i} n(\mathbf{r}, t) \, \Delta V \quad (2)$$

where $r_i = i \Delta r$ ranges from 0 to 10 a_0 and ΔV is the volume of each grid cell. We then fit the resulting radial distribution to

a linear combination of analytic radial distributions of hydrogen orbitals (1s, 2s, and 2p) and a uniform background density to account for nearby free electrons. The resulting fits capture the numerically calculated radial distributions extremely well (see Fig. 2), with R^2 values generally above 0.9. In Ref. [58], we show that the DFT orbitals of an isolated H^+ ion closely match the analytical hydrogen orbitals (see Fig. S4) and that including even higher energy orbitals has a negligible effect
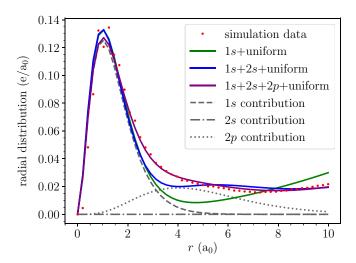

FIG. 2. Curve fitting used to determine the orbital occupations of the proton projectile and to calculate the charge it captured. Red circles show simulation results for the radial distribution of the electron density around the projectile (1 at. u. of velocity) 1.2 fs after it exits from a four-layer aluminum sheet. Least squares fits to this data using different analytic hydrogen orbitals and a uniform background charge are shown in green, blue, and purple. Radial distributions for analytic 1s, 2s, and 2p hydrogen orbitals are shown in gray; they are scaled by their respective occupations as obtained from the 1s + 2s + 2p + uniform fit, which describes the simulation results very well.

on the orbital occupations and the total charge transfer (see Fig. S5).

Finally, in order to analyze plasma oscillations induced in the aluminum sheet, we compute the out-of-plane dipole moment

$$d(t) = \int_V z \, n(\mathbf{r}, t) \, dr^3, \tag{3}$$

where $\hat{z}$ is normal to the aluminum surface and V is the volume occupied by the sheet. In order to account for the electron density extending from the aluminum surface, we include within V the region within 11 a_0 of the aluminum surface atoms (see yellow dashed lines in Fig. 1). Using this cutoff gives less than 6×10^{-3} electrons in the vacuum at the start of each calculation.

IV. RESULTS AND DISCUSSION

A. Pre-equilibrium electronic stopping

A fast projectile impacting a *bulk* target or sufficiently thick foil reaches an equilibrium charge state within a few fs and within the first few nm of material traversed [13,14]. The projectile then experiences equilibrium electronic stopping [77], and as a result its velocity decreases over a time scale much longer than the initial charge equilibration. As the projectile slows down, its equilibrium charge state also evolves as a function of velocity. However, the situation is more complicated for thin target materials. Upon approaching and entering the surface, an ion dynamically captures or loses electrons [78], leading to energy transfer dynamics which have been detected as a dependence of stopping power in thin foils on the initial charge state of the projectile [79]. This pre-equilibrium behavior in the projectile charge and stopping power within the material surface would then also influence surface processes such as electron emission.

Our results show clear pre-equilibrium effects in the energy transferred from the projectile to the host material from the comparison of the stopping power in thin aluminum sheets to bulk aluminum: Figure 3 shows 13–25% greater stopping, depending on projectile velocity and sheet thickness, for H$^+$ in the aluminum sheets compared to theoretical [26] and empirically fitted [80] results for H in bulk aluminum. Since the stopping powers of H and H$^+$ in bulk aluminum quickly converge toward the same value [26], this comparison isolates surface effects in the host material. Furthermore, the inset of Fig. 3 shows that the stopping power varies with sheet thickness and does not approach the bulk value even for a 12-layer sheet, the thickest one we simulated.

In order to explain why pre-equilibrium stopping is larger than bulk stopping, we first analyze the projectile charge state dynamics. This allows us to compare to analytic models that predict that stopping power varies quadratically with projectile charge [7–11]. Interestingly, we find from Fig. 4 that the instantaneous projectile charge state as calculated by the DDEC6 method [70,71] is actually anticorrelated with the instantaneous stopping power: The proton experiences enhanced stopping despite lower effective charge within the first few atomic layers, and the fluctuations arising from lattice periodicity are out of phase, with local maxima in stopping power aligned with local minima in effective charge state and
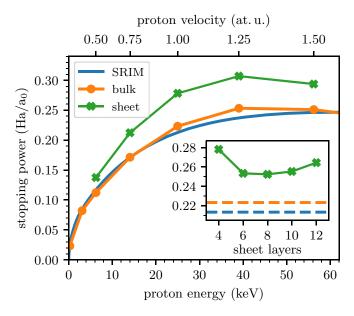

FIG. 3. Electronic stopping as a function of kinetic energy of a proton projectile in a four-layer aluminum sheet (green) is higher than in bulk aluminum (TDDFT results [26] in orange and SRIM data [80] in blue). Inset: Electronic stopping of a 25 keV proton (velocity of 1 at. u.) for different aluminum sheet thicknesses. Dashed lines indicate bulk values from TDDFT [26] (orange) and SRIM [80] (blue). For each sheet, average stopping is computed across the two middle layers as the most bulklike region.

vice versa. Thus, the dynamical behavior of the projectile charge state appears incompatible with equilibrium stopping power models and does not explain the pre-equilibrium stopping behavior near the material's surface. However, we also note that charge partitioning schemes may not be capable
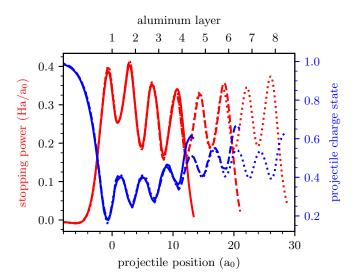

FIG. 4. Instantaneous electronic stopping (red) and effective projectile charge state from DDEC6 analysis [70,71] analysis (blue) for a proton projectile with 1 at. u. of velocity traversing aluminum sheets that are four, six, and eight layers thick (solid, dashed, dotted, respectively). The entrance layer of aluminum atoms is located at 0 a_0.
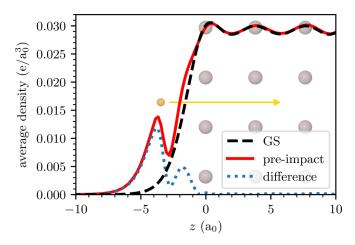
FIG. 5. Average electron density located within a 1 a_0 radius of the proton's trajectory for the ground-state initial condition (dashed black) and when the proton, approaching with 1 at. u. of velocity, is 3.5 a_0 away from impacting a four-layer aluminum sheet (solid red). Dotted blue shows the difference between the average densities just before impact and in the ground state. The positions of the aluminum atoms (proton projectile) are indicated in gray (gold).
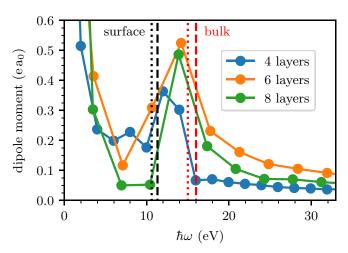

FIG. 6. Fourier transform of the time-dependent out-of-plane dipole moment in the aluminum sheets after impact by a proton with 1 at. u. of velocity. Only data at least 0.7 fs after the projectile exits the material was analyzed in order to isolate plasma oscillations and exclude contributions from emitted electrons. The dashed (dotted) lines indicate the theoretical (experimental) energies of the bulk and surface plasmons [81–83].

of accurately resolving the relatively small changes in the charge state occurring here, as the captured electron density is superimposed with the projectile's wake in the host material.

Another potential source of enhanced pre-equilibrium stopping, according to analytic models [7–10], would be higher electron density near the entrance surface. We indeed observe such higher electron density, arising from the polarization induced on the aluminum sheet during the proton's approach (see Fig. 5). However, we found that before impact, this polarization is highly localized to the very surface, without extending into the first two atomic layers where the enhanced stopping is observed. Once the projectile enters the material, it again becomes impossible to disentangle its wake from its captured electrons. Therefore, we cannot definitively attribute the enhanced surface stopping power to surface polarization.

Finally, the higher stopping may be explained by surface or confinement effects of thin sheets: Aluminum surfaces have an additional excitation channel in the form of surface plasmons. In addition, the plasmonic behavior of atomically thin metal films has been shown to deviate from bulk [84] and predicted to support multiple surface, subsurface, and bulk plasmon modes [85]. Surface plasmon modes have indeed been predicted to become increasingly important and lead to higher stopping power for incident electrons as film thickness is reduced [86]. To investigate this mechanism, we performed a Fourier analysis of the time-dependent out-of-plane dipole moment, Eq. (3), and we indeed found indications for plasmon modes located between the bulk and surface plasmon energies (see Fig. 6). While our frequency resolution is fairly low due to the few-fs time scale of our simulations, Fig. 6 shows that the data for the four-layer sheet hints at the possibility of two distinct plasmon peaks. Future studies with significantly longer total propagation time would be needed to unambiguously distinguish specific bulk and surface modes. Nonetheless, surface plasmon excitations and/or nonbulk plasmonic

behavior represent plausible mechanisms for enhanced electronic stopping near an aluminum surface.

We also note that the de Broglie wavelength of electrons at the Fermi surface in aluminum (6.8 a_0) is comparable to the thickness of the aluminum sheets (15–92 a_0), suggesting that quantum confinement may affect the thinner sheets studied. However, since the instantaneous stopping power remains almost identical for sheets with different thicknesses until the projectile reaches the exit surface (see Fig. 4), we conclude that any quantum confinement effects do not significantly influence electronic stopping power in this system.

B. Projectile charge capture

Experimental studies often infer information about pre-equilibrium behavior from charge state distributions of the projectile after transmission through a foil [14–16,87,88]. Thus, we calculated the number of electrons captured by the projectile after emerging from the aluminum sheets by analyzing the electron density as described in Sec. III. Our method also provides information about the sub-fs real-time dynamics of orbital occupations of the captured electrons.

First, we found that charge captured by the projectile remains nearly constant as a function of aluminum sheet thickness [see Fig. 7(a)] but decreases with higher proton velocity across the entire velocity range considered [see Fig. 7(b)]. The majority of the captured electron density occupies the $1s$ orbital, with a smaller portion occupying the $2s$ and $2p$ orbitals. Figure 7(b) also shows that the $2s$ and $2p$ orbital occupation is largely independent of the velocity and the change in total captured charge can be attributed to the $1s$ shell of the projectile. Hence, while slower projectiles capture more charge from the target and are close to their $1s$ ground state, faster projectiles capture less charge but any captured electrons are more likely to occupy an excited state.
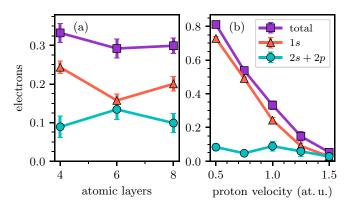
FIG. 7. (a) Total charge captured by the projectile, decomposed into occupations of the $1s$ and $2s + 2p$ hydrogen orbitals, after a proton with 1 at. u. of velocity impacts aluminum sheets of different thickness. Error bars indicate standard deviations of these time-dependent values. (b) The same quantities are shown as a function of projectile velocity for protons impacting four-layer aluminum.
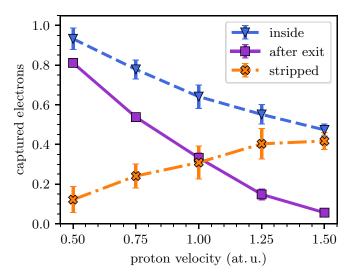

FIG. 8. Average number of electrons captured by the proton projectile inside (blue triangles) and after exiting (purple squares) a four-layer aluminum sheet. The difference between these two quantities, the number of electrons stripped at the exit-side surface, is shown in orange exes. Error bars indicate standard deviations of the time-dependent quantities.

The lack of dependence of charge capture on sheet thickness [see Fig. 7(a)] is surprising given the pre-equilibrium stopping presented in Sec. IV A. In particular, this behavior is a departure from experiments employing heavier/higher charge projectiles which observed that charge transfer distributions depend on foil thickness [14,87]. Thus, our results indicate that light ions can experience pre-equilibrium stopping power even after projectile charge equilibration. This conclusion is further supported by the finding that the projectile's charge almost reaches equilibrium even within the thinnest sheet studied here (see Fig. 4) despite pre-equilibrium stopping power even for the thickest sheets (see inset of Fig. 3). Furthermore, this supports our interpretation that larger pre-equilibrium stopping for light ions is related to the target material, via its surface plasmons, rather than being a property of the projectile charge state.

We also note another interesting surface effect: The projectile emerges with a higher exit charge state than its effective charge state within the sample. Our data shows this for a proton with a velocity of 1 at. u., which equilibrates to a charge of about 0.5 *within* the eight-layer sheet (see Fig. 4), but retains only about 0.3 electrons when it *exits* with a charge of 0.7 (see Fig. 7). These findings indicate that the exit-side surface strips a portion of electrons that had been captured within the material, an effect not described by existing models of projectile charge equilibration [14,18]. We find that the number of electrons that are stripped at the surface increases with proton velocity (see Fig. 8). These discrepancies between the projectile's charge state within the material and after exiting into the vacuum lead us to advise caution in drawing conclusions about pre-equilibrium behavior from measurements of only the projectile's exit charge state.

Finally, our analysis of the femtosecond dynamics of projectile orbital occupations shows that for $v \gtrsim 0.75$ at. u., the captured electrons fluctuate between the $1s$ and $2s/2p$ states. We show this explicitly for $v = 1.0$ at. u. in Fig. 9, and the oscillatory behavior for $v = 1.25$ at. u. and 1.5 at. u. is similar (see Fig. S7 of Ref. [58]). The Fourier transform of the time-dependent $1s$ occupation number features a strong peak

at a frequency ranging from $\hbar\omega = 10.5 \pm 1.3$ eV to 11.7 ± 1.2 eV, depending on projectile velocity and sheet thickness. Since these oscillation frequencies lie near the 10.2 eV energy difference between the $n = 1$ and $n = 2$ hydrogen orbitals, the fluctuations with these frequencies suggest a superposition of these two states. We also note that for a projectile velocity of $v = 0.75$ at. u., the amplitude of the oscillations in the orbital occupation dynamics becomes very small, making them hard to interpret, and at lower velocities the oscillations disappear (see Fig. S8 of Ref. [58]). In this low velocity regime, occupation of the $1s$ orbital dominates. This again indicates that slower projectiles are much closer to their electronic ground state when exiting the aluminum sheet.
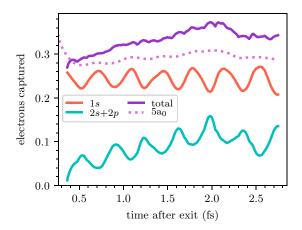

FIG. 9. Time-dependent hydrogen orbital occupations after a proton projectile with 1 at. u. of velocity traverses a four-layer aluminum sheet. The number of electrons within 5 a_0 of the projectile is included for reference.

V. CONCLUSIONS

Our first-principles simulations of proton-irradiated aluminum sheets revealed detailed information about pre-equilibrium stopping power near a metal's surface. We found higher average stopping power in the aluminum sheets compared to bulk aluminum and a pronounced stopping power enhancement within the entrance layers. These deviations from bulk behavior are not adequately explained by pre-equilibrium projectile charge, surface polarization, or quantum confinement; the most viable mechanism for surface stopping enhancement is surface plasmon excitations.

We also presented a technique based on analytical hydrogen orbitals to extract from the electron density not only the exit charge state of the projectile but also the orbital occupations of the captured electrons. The electrons captured by the proton predominantly occupy the $1s$ orbital, though for higher velocities the projectile emerges in a superposition of $1s$ and $2s/2p$ orbitals. Moreover, the projectile's exit charge state differs from its equilibrium charge within the material, and the number of electrons stripped from the projectile as it emerges from the exit-side surface increases with projectile velocity.

This work provides details about pre-equilibrium behavior in ion-irradiated surfaces and thin materials, offering unprecedented insight into the few-fs dynamics of electronic stopping power and projectile charge equilibration. This study also has broad implications for advancing radiation hardness and ion beam techniques for imaging, defect engineering, and nanostructuring, as these applications are chiefly concerned with energy deposition near material surfaces. The electron density analysis framework developed in this work lays the foundation for further computational research on charge dynamics near ion-irradiated surfaces and 2D materials.

Inputs and outputs from our simulations are available at the Materials Data Facility [89,90].

[1] J. Notte, B. Ward, N. Economou, R. Hill, R. Percival, L. Farkas, and S. McVey, in *Characterization and Metrology for Nanoelectronics: 2007 International Conference on Frontiers of Characterization and Metrology*, edited by D. G. Seiler, A. C. Diebold, R. McDonald, C. M. Garner, D. Herr, R. P. Khosla, and E. M. Secula, AIP Conf. Proc. No. 931 (AIP, New York, 2007), p. 489.

[2] I. Utke, P. Hoffmann, and J. Melngailis, J. Vac. Sci. Technol. B **26**, 1197 (2008).

[3] R. Ritter, R. A. Wilhelm, M. Stöger-Pollach, R. Heller, A. Mücklich, U. Werner, H. Vieker, A. Beyer, S. Facsko, A. Gölzhäuser, and F. Aumayr, Appl. Phys. Lett. **102**, 063112 (2013).

[4] G. Hlawacek, V. Veligura, R. van Gastel, and B. Poelsema, J. Vac. Sci. Technol. B **32**, 020801 (2014).

[5] D. S. Fox, Y. Zhou, P. Maguire, A. O'Neill, C. Ó'Coileáin, R. Gatensby, A. M. Glushenkov, T. Tao, G. S. Duesberg, I. V. Shvets, M. Abid, M. Abid, H.-C. Wu, Y. Chen, J. N. Coleman, J. F. Donegan, and H. Zhang, Nano Lett. **15**, 5307 (2015).

[6] Z. Li and F. Chen, Appl. Phys. Rev. **4**, 011103 (2017).

[7] H. Bethe, Ann. Phys. **397**, 325 (1930).

[8] P. Sigmund, *Particle Penetration and Radiation Effects: General Aspects and Stopping of Swift Point Charges*, Springer Series in Solid-State Science Vol. 151 (Springer, Berlin, Heidelberg, 2006).

[9] E. Fermi and E. Teller, Phys. Rev. **72**, 399 (1947).

[10] J. Lindhard and A. Winther, Matemat.-Fysis. Meddel. **34**, 1 (1964).

[11] P. Wang, T. M. Mehlhorn, and J. J. MacFarlane, Phys. Plasmas **5**, 2977 (1998).

[12] A. A. Correa, Comput. Mater. Sci. **150**, 291 (2018).

[13] C.-W. Lee, J. A. Stewart, S. M. Foiles, R. Dingreville, and A. Schleife, Phys. Rev. B **102**, 024107 (2020).

[14] M. Hattass, T. Schenkel, A. V. Hamza, A. V. Barnes, M. W. Newman, J. W. McDonald, T. R. Niedermayr, G. A. Machicoane, and D. H. Schneider, Phys. Rev. Lett. **82**, 4795 (1999).

[15] R. A. Wilhelm, E. Gruber, R. Ritter, R. Heller, S. Facsko, and F. Aumayr, Phys. Rev. Lett. **112**, 153201 (2014).

[16] T. Schenkel, M. A. Briere, H. Schmidt-Böcking, K. Bethge, and D. H. Schneider, Phys. Rev. Lett. **78**, 2481 (1997).

[17] H. L. Sun, Y. C. Yu, E. K. Lin, C. W. Wang, J. L. Duggan, A. R. Azordegan, F. D. McDaniel, and G. Lapicki, Phys. Rev. A **53**, 4190 (1996).

[18] W. Brandt, R. Laubert, M. Mourino, and A. Schwarzschild, Phys. Rev. Lett. **30**, 358 (1973).

[19] R. A. Wilhelm, E. Gruber, J. Schwestka, R. Kozubek, T. I. Madeira, J. P. Marques, J. Kobus, A. V. Krasheninnikov, M. Schleberger, and F. Aumayr, Phys. Rev. Lett. **119**, 103401 (2017).

[20] R. A. Wilhelm, E. Gruber, J. Schwestka, R. Heller, S. Fascko, and F. Aumayr, Appl. Sci. **8**, 1050 (2018).

[21] P. Koschar, K. Kroneberger, A. Clouvas, M. Burkhard, W. Meckbach, O. Heil, J. Kemmler, H. Rothard, K. O. Groeneveld, R. Schramm, and H.-D. Betz, Phys. Rev. A **40**, 3632 (1989).

[22] P. Mertens and T. Krist, Nucl. Instrum. Methods Phys. Res. **194**, 57 (1982).

[23] D. Semrad, P. Mertens, and P. Bauer, Nucl. Instrum. Methods Phys. Res., Sect. B **15**, 86 (1986).

[24] S. P. Møller, A. Csete, T. Ichioka, H. Knudsen, U. I. Uggerhøj, and H. H. Andersen, Phys. Rev. Lett. **93**, 042502 (2004).

[25] A. A. Correa, J. Kohanoff, E. Artacho, D. Sánchez-Portal, and A. Caro, Phys. Rev. Lett. **108**, 213201 (2012).

[26] A. Schleife, Y. Kanai, and A. A. Correa, Phys. Rev. B **91**, 014306 (2015).

[27] E. E. Quashie, B. C. Saha, and A. A. Correa, Phys. Rev. B **94**, 155403 (2016).

[28] M. Caro, A. A. Correa, E. Artacho, and A. Caro, Sci. Rep. **7**, 2618 (2017).

[29] R. Ullah, E. Artacho, and A. A. Correa, Phys. Rev. Lett. **121**, 116401 (2018).

[30] A. Lim, W. M. C. Foulkes, A. P. Horsfield, D. R. Mason, A. Schleife, E. W. Draeger, and A. A. Correa, Phys. Rev. Lett. **116**, 043201 (2016).

[31] D. C. Yost and Y. Kanai, Phys. Rev. B **94**, 115107 (2016).

[32] D. C. Yost, Y. Yao, and Y. Kanai, Phys. Rev. B **96**, 115134 (2017).

[33] C.-W. Lee and A. Schleife, Eur. Phys. J. B **91**, 222 (2018).

[34] K. Kang, A. Kononov, C.-W. Lee, J. A. Leveillee, E. P. Shapera, X. Zhang, and A. Schleife, Comput. Mater. Sci. **160**, 207 (2019).

[35] C.-W. Lee and A. Schleife, Nano Lett. **19**, 3939 (2019).

[36] J. M. Pruneda, D. Sánchez-Portal, A. Arnau, J. I. Juaristi, and E. Artacho, Phys. Rev. Lett. **99**, 235501 (2007).

[37] F. Mao, C. Zhang, J. Dai, and F.-S. Zhang, Phys. Rev. A **89**, 022707 (2014).

[38] C.-K. Li, F. Wang, B. Liao, X.-P. OuYang, and F.-S. Zhang, Phys. Rev. B **96**, 094301 (2017).

[39] M. Peñalba, A. Arnau, P. M. Echenique, F. Flores, and R. H. Ritchie, Europhys. Lett. (EPL) **19**, 45 (1992).

[40] M. Quijada, A. G. Borisov, I. Nagy, R. Diez Muiño, and P. M. Echenique, Phys. Rev. A **75**, 042902 (2007).

[41] M. A. Zeb, J. Kohanoff, D. Sánchez-Portal, and E. Artacho, Nucl. Instrum. Methods Phys. Res., Sect. B **303**, 59 (2013), proceedings of the 11th Computer Simulation of Radiation Effects in Solids (COSIRES) Conference Santa Fe, New Mexico, USA, July 24-29, 2012.

[42] E. Runge and E. K. U. Gross, Phys. Rev. Lett. **52**, 997 (1984).

[43] M. Marques and E. Gross, Annu. Rev. Phys. Chem. **55**, 427 (2004).

[44] M. Marques, *Time-Dependent Density Functional Theory* (Springer Science & Business Media, Berlin, Heidelberg, 2006).

[45] C. A. Ullrich, *Time-Dependent Density-Functional Theory: Concepts and Applications* (Oxford University Press, New York, 2012).

[46] C. A. Ullrich and Z.-h. Yang, Braz. J. Phys. **44**, 154 (2014).

[47] A. Schleife, E. W. Draeger, Y. Kanai, and A. A. Correa, J. Chem. Phys. **137**, 22A546 (2012).

[48] A. Schleife, E. W. Draeger, V. Anisimov, A. A. Correa, and Y. Kanai, Comput. Sci. Eng. **16**, 54 (2014), special issue on "Leadership Computing".

[49] F. Gygi, IBM J. Res. Dev. **52**, 137 (2008).

[50] E. W. Draeger and F. Gygi, "Qbox code, qb@ll version", https://github.com/LLNL/qball, (2017), Lawrence Livermore National Laboratory.

[51] N. Troullier and J. L. Martins, Phys. Rev. B **43**, 1993 (1991).

[52] D. Vanderbilt, Phys. Rev. B **32**, 8412 (1985).

[53] A. Zangwill and P. Soven, Phys. Rev. Lett. **45**, 204 (1980).

[54] A. Zangwill and P. Soven, Phys. Rev. B **24**, 4121 (1981).

[55] S. Zhao, W. Kang, J. Xue, X. Zhang, and P. Zhang, J. Phys.: Condens. Matter **27**, 025401 (2015).

[56] A. Castro, M. A. L. Marques, and A. Rubio, J. Chem. Phys. **121**, 3425 (2004).

[57] E. W. Draeger, X. Andrade, J. A. Gunnels, A. Bhatele, A. Schleife, and A. A. Correa, J. Parallel Distr. Com. **106**, 205 (2017).

[58] See Supplemental Material at http://link.aps.org/supplemental/10.1103/PhysRevB.102.165401 for details regarding time evolution accuracy, convergence of supercell dimensions, validation of our method to calculate charge captured by the projectile including comparison to volume and charge partitioning, and additional results for time-dependent projectile orbital occupations.

[59] R. S. Mulliken, J. Chem. Phys. **23**, 1833 (1955).

[60] O. Knospe, J. Jellinek, U. Saalmann, and R. Schmidt, Eur. Phys. J. D **5**, 1 (1999).

[61] O. Knospe, J. Jellinek, U. Saalmann, and R. Schmidt, Phys. Rev. A **61**, 022715 (2000).

[62] C. M. Isborn, X. Li, and J. C. Tully, J. Chem. Phys. **126**, 134307 (2007).

[63] Y. Miyamoto and H. Zhang, Phys. Rev. B **77**, 161402(R) (2008).

[64] P.-G. Reinhard and E. Suraud, J. Cluster Sci. **10**, 239 (1999).

[65] C. A. Ullrich, J. Mol. Struct (THEOCHEM) **501-502**, 315 (2000).

[66] F. Wang, X. C. Xu, X. H. Hong, J. Wang, and B. C. Gou, Phys. Lett. A **375**, 3290 (2011).

[67] F. Wang, X. H. Hong, J. Wang, B. C. Gou, and J. G. Wang, Phys. Lett. A **376**, 469 (2012).

[68] C.-Z. Gao, J. Wang, and F.-S. Zhang, Chem. Phys. **410**, 9 (2013).

[69] R. F. W. Bader, *Atoms in Molecules: A Quantum Theory* (Clarendon Press, Oxford, 1994).

[70] T. A. Manz and N. G. Limas, RSC Adv. **6**, 47771 (2016).

[71] N. Gabaldon Limas and T. A. Manz, RSC Adv. **6**, 45727 (2016).

[72] P. Reinhard, E. Suraud, and C. Ullrich, Eur. Phys. J. D **1**, 303 (1998).

[73] Y. Miyamoto and H. Zhang, Phys. Rev. B **77**, 045433 (2008).

[74] G. Avendano-Franco, B. Piraux, M. Grüning, and X. Gonze, Theor. Chem. Acc. **131**, 1289 (2012).

[75] F. Mao, C. Zhang, C.-Z. Gao, J. Dai, and F.-S. Zhang, J. Phys.: Condens. Matter **26**, 085402 (2014).

[76] A. Ojanperä, A. V. Krasheninnikov, and M. Puska, Phys. Rev. B **89**, 035120 (2014).

[77] R. Herrmann, C. L. Cocke, J. Ullrich, S. Hagmann, M. Stoeckli, and H. Schmidt-Boecking, Phys. Rev. A **50**, 1435 (1994).

[78] N. Bohr, *The Penetration Atomic Particles Through Matter* (The Royal Danish Academy of Science, Copenhagen, 1948).

[79] H. Ogawa, I. Katayama, I. Sugai, Y. Haruyama, M. Saito, K. Yoshida, M. Tosaki, and H. Ikegami, Nucl. Instrum. Methods Phys. Res., Sect. B **82**, 80 (1993).

[80] J. F. Ziegler, M. D. Ziegler, and J. P. Biersack, Nucl. Instrum. Methods Phys. Res., Sect. B **268**, 1818 (2010), 19th International Conference on Ion Beam Analysis.

[81] D. Pines, Rev. Mod. Phys. **28**, 184 (1956).

[82] C. J. Powell and J. B. Swan, Phys. Rev. **115**, 869 (1959).

[83] G. Grosso and G. P. Parravicini, in *Solid State Physics*, 2nd ed. (Academic Press, Amsterdam, 2014), pp. 287–331.

[84] R. A. Maniyara, D. Rodrigo, R. Yu, J. Canet-Ferrer, D. S. Ghosh, R. Yongsunthon, D. E. Baker, A. Rezikyan, F. J. García de Abajo, and V. Pruneri, Nat. Photonics **13**, 328 (2019).

[85] K. Andersen, K. W. Jacobsen, and K. S. Thygesen, Phys. Rev. B **86**, 245129 (2012).

[86] R. H. Ritchie, Phys. Rev. **106**, 874 (1957).

[87] A. Bürgi, M. Gonin, M. Oetliker, P. Bochsler, J. Geiss, T. Lamy, A. Brenac, H. J. Andrä, P. Roncin, H. Laurent, and M. A. Coplan, J. Appl. Phys. **73**, 4130 (1993).

[88] L. Folkerts, S. Schippers, D. M. Zehner, and F. W. Meyer, Phys. Rev. Lett. **74**, 2204 (1995).

[89] B. Blaiszik, K. Chard, J. Pruyne, R. Ananthakrishnan, S. Tuecke, and I. Foster, JOM **68**, 2045 (2016).

[90] A. Kononov and A. Schleife, Dataset for 'pre-equilibrium stopping and charge capture in proton-irradiated aluminum sheets', https://www.doi.org/10.18126/4ene-mwpd (2020).